2024 European Control Conference (ECC)
June 25-28, 2024. Stockholm, Sweden

Fast determination of OCV curve for Lithium-ion batteries*

Maxime Bussios[1], Alejandro Goldar[1], Emanuele Garone[1] and Michel Kinnaert[1]

Abstract— **The open circuit voltage (OCV) is a chemistry-dependent curve that characterizes the steady-state behaviour of a lithium-ion battery cell (LIB), namely the link between the voltage accross the cell and its state of charge (SOC), when no load is connected. It is a fundamental ingredient to estimate the SOC of LIBs with any technique, ranging from a simple look-up table to a Kalman filter based on an equivalent circuit model or an electrochemical model. However, an accurate determination of such a steady-state curve for a commercial LIB requires extensive standalone experimental campaigns that are time-consuming. This work, compares two different methods, Karhunen-Loève transform (or principal component analysis) and Gaussian process regressions, to model the zero-current behaviour of 18650 LIBs (Sony VTC6 and Samsung 30Q, 3000mAh) considering OCV-SOC charge and discharge experimental curves at C-rates between C/50 and C/5. The zero-current extrapolation given by these methods can reduce the experimental time up to 85% when compared to an average OCV characterized at C/100.**

I. Introduction

Lithium-ion batteries have become ubiquitous energy storage solutions, powering an array of applications from portable electronic devices to electric vehicles and renewable energy systems. Their versatility and high energy density have made them the preferred choice for many modern technologies. To fully harness the potential of lithium-ion batteries and optimize their performance, accurate State of Charge (SOC) monitoring has emerged as a central concern. The SOC of a battery indicates the amount of energy stored in the battery with respect to its nominal capacity. Monitoring SOC in real-time is essential for a multitude of reasons, including ensuring the safety, extending the lifespan, and optimizing the energy utilization of lithium-ion batteries. The relationship between the open circuit voltage (OCV) and the SOC, namely the $\mathrm{OCV}-\mathrm{SOC}$ curve, is a key ingredient for battery SOC estimation. This curve allows for the estimation of the current SOC based on measured terminal voltage by inverting the relationship. This process is often augmented with the use of state observers to mitigate errors arising from transient effects, measurement noise and curve plateaus. Extended Kalman filters (EKF) as well as other observers, such as Luenberger observers, adaptive observers, etc. are built on the basis of the $\mathrm{OCV}-\mathrm{SOC}$ relationship and an electrochemical or an equivalent circuit model (ECM) to estimate the SOC. Sometimes the state of health (SOH) of the battery is also estimated [1]. For example, in [2], an extended Kalman filter (EKF) is used to provide an estimation of the SOC from the voltage and current measurements, and an electrochemical model involving the $\mathrm{OCV}-\mathrm{SOC}$ curve of each electrode. In [3], the authors used the OCV-SOC relationship in a non-linear observer whose design relies on linear matrix inequalities (LMI) in order to estimate the state of individual cells in a battery pack. In [4], the SOC and the SOH are jointly estimated, using two EKF with different time scales. These filters rely on ECMs involving an OCV-SOC function.

However, the acquisition of the OCV curve is a time-consuming task. Given that the OCV, by definition, characterizes the steady-state voltage when no current passes through the battery, experiments for obtaining this curve necessitate either to conduct tests at very low currents [5] or to employ extensive relaxation period, spanning the entire SOC range from 0% to 100% [6] [7]. A frequently employed method [6] [7] for obtaining the OCV curve is the voltage relaxation approach. In this method, a brief current pulse is applied, typically causing a minor SOC change, after which the battery is allowed to rest for a period of 5-6 hours, for relaxation. Afterward, voltage measurements are taken, and this process is iteratively repeated until the entire SOC range is explored. Another common approach [5][8][9][10][11] consists in recording the voltage versus SOC curves for charge/discharge experiments at very low current. Indeed, low current allows reducing the impact of overpotential and ohmic effects on the terminal voltage [5]. However, a persistent challenge lies in the hysteresis observed between the curves acquired during charging and discharging [12][13][14]. Even though neglecting this phenomenon induces an error, typical application-oriented estimators adopt a unified model for all battery operations. In this scenario, the average of the voltage values measured at the same SOC during charging and discharging at low C-rate is performed. The resulting averaged curve is then considered as the OCV curve [5] [6].

The objective of this study is to develop a faster approach for determining the OCV curve than the aforementioned methods, while maintaining the prediction error within the same order of magnitude as the one arising from the above-mentioned averaging process.

II. Proposed methods

The two methods presented hereunder consist in performing charge/discharge experiments at different constant C-rates[1] The corresponding voltage (V) versus SOC curves are

*This work is supported by the Fonds de la Recherche Scientifique – FNRS under grants T.0142.20 and 4008266 and by the Walloon Region through project BATFACTORY

[1]Service d'automatique et d'analyse des systèmes, Université Libre de Bruxelles, Av. Franklin Roosevelt 50, CP 165/55, 1050, Brussels - Belgium,

[1]A C-rate of 1C corresponds to the current needed to fully charge/discharge a battery in one hour.

then modeled and extrapolated to a zero current condition. The first approach involves expanding the signals as a weighted sum of basis vectors and extrapolating the weights. It extrapolates the voltage versus SOC curve for charge and discharge separately and then take the average of the resulting two curves. The second approach treats the signals at different C-rates, taking into consideration charge and discharge conjointly, as a function of two variables (current and SOC) and extrapolates this function to zero current.

A. Karhunen-Loève transform or principal component analysis

The methodology presented in this section replicates the work conducted by [7]. The reproduction of this work serves two purposes : firstly, to compare the outcomes of this promising approach with the other method and secondly, to evaluate its performance in the more nonlinear sections of the OCV curve (0%-30% and 70%-100%), where the original study [7] lacks experimental data.

Consider an $m \times n$ matrix $\mathbf{V}$ of voltage measurements. Each row corresponds to a different charging or discharging currents, $I_j, j = 1, \ldots, m$ in the range [0.02,0.2] expressed in terms of C-rate (I_j=0.1 corresponds to a C-rate of C/10). Each row is made of n measurements associated to equidistant SOC values in the range [0,1]. Typically $n > m$ in the considered situation. The Karhunen-Loève transform is equivalent to principal component analysis (PCA). It is a data reduction method that is optimal in the mean square sense and aims at eliminating the effect of noise in the data set. More precisely, a p-dimensional subspace, $\mathcal{W} \subset R^n$ is sought such that

$$\sum_{\ell=1}^{m} \|\mathbf{V}(\ell, \cdot) - P_{\mathcal{W}}(\mathbf{V}(\ell, \cdot))\|^2 \tag{1}$$

is minimum. Here $P_{\mathcal{W}}(\mathbf{V}(\ell, \cdot))$ stands for the projection of the ℓ^{th} row of matrix $\mathbf{V}$, denoted $\mathbf{V}(\ell, \cdot)$, in the subspace $\mathcal{W}$. It turns out that a basis for subspace $\mathcal{W}$ can be determined by computing the eigenvalues of the so-called scatter matrix defined as

$$\mathbf{S} = \sum_{\ell=1}^{m} (\mathbf{V}(\ell, \cdot) - \mu)^T (\mathbf{V}(\ell, \cdot) - \mu)$$

where $\mu = \frac{1}{m} \sum_{\ell=1}^{m} \mathbf{V}(\ell, \cdot)$ is the empirical mean over the rows of matrix $\mathbf{V}$. Equivalently, such a basis can also be determined by a singular value decomposition of

$$\tilde{\mathbf{V}} = \mathbf{V} - [1\ 1 \ldots 1]^T \otimes \mu$$

where $\otimes$ stands for the Kronecker product. Indeed, letting the singular value decomposition of $\tilde{\mathbf{V}}$ be

$$\tilde{\mathbf{V}} = \mathbf{U}\mathbf{\Sigma}\mathbf{W}^T \tag{2}$$

where $\mathbf{U}$ and $\mathbf{W}$ are orthogonal matrices with dimension $m \times m$ and $n \times n$ respectively and $\mathbf{\Sigma}$ is an $m \times n$ matrix of the form $[diag\{\sigma_1 \ldots \sigma_m\}\ \ \mathbf{0}]$ where $\sigma_1 > \sigma_2 > \ldots \sigma_m > 0$ are the singular values of $\tilde{\mathbf{V}}$ and $\mathbf{0}$ stands for the $m \times (n-m)$ zero matrix. A basis for the p-dimensional subspace $\mathcal{W}$ is made of the first p columns of W and the reduced data matrix is given as

$$\tilde{\mathbf{V}}_p = \mathbf{U}_p \mathbf{\Sigma}_p \mathbf{W}_p^T \tag{3}$$

where $\mathbf{U}_p$ is made of the first p columns of $\mathbf{U}$ and $\mathbf{\Sigma}_p = diag\{\sigma_1 \ldots \sigma_p\}$. Equivalently, equation (3) can be rewritten

$$\tilde{\mathbf{V}}_p = \sum_{j=1}^{p} \mathbf{A}(\cdot, j) \mathbf{W}_p(\cdot, j)^T \tag{4}$$

where $\mathbf{A} = \mathbf{U}_p \mathbf{\Sigma}_p$. It has been observed in [7] that the elements $a_{i,j}$ of $\mathbf{A}(\cdot, j)$ can be approximately described by an affine function of the current of the form $a_{i,j} \approx \alpha_j + \beta_j I_i$ for sufficiently low currents. The corresponding coefficients α_j and β_j, $j = 1, \ldots, p$ can be found by least squares parameter estimation. An approximate OCV curve can then be obtained by extrapolating these functions for $I = 0$. The resulting OCV estimate, denoted $\widehat{OCV}$, can be deduced as:

$$\widehat{OCV} = \sum_{j=1}^{p} \alpha_j \mathbf{W}_p(\cdot, j)^T$$

Each element of this row vector corresponds to one of the equidistant SOC values at which the voltage measurements were taken.

B. Gaussian process regression method

Our aim is to estimate a function, $f(SOC, I)$ that models the recorded voltage curves for each current values, $I_j, j = 1, \ldots, m$. We choose function f to be described by a Gaussian process (GP) for the flexibility of this tool to approximate functions and for the limited number of design parameters involved in Gaussian process regression.

Letting $\mathbf{x} = [SOC, I]^T$, by definition of a Gaussian process, for any set of input points $\{\mathbf{x}_i, i = 1, \ldots, s\}$ (which can be concatenated into a $2 \times s$ matrix, $\mathbf{X}$) the vector $\mathbf{f}$ defined as

$$\mathbf{f} = [f(\mathbf{x}_1) \ldots f(\mathbf{x}_s)]^T$$

follows a multivariate Gaussian distribution, namely $\mathcal{N}(\mathbf{m_f}(\mathbf{X}), \mathbf{K_f}(\mathbf{X}, \mathbf{X}))$. The mean and covariance of $\mathbf{f}$ respectively take the form

$$\mathbf{m_f}(\mathbf{X}) = \begin{bmatrix} m(\mathbf{x}_1) \\ \vdots \\ m(\mathbf{x}_s) \end{bmatrix}.$$

$$\mathbf{K_f}(\mathbf{X}, \mathbf{X}) = \begin{bmatrix} k(\mathbf{x}_1, \mathbf{x}_1) \ldots k(\mathbf{x}_1, \mathbf{x}_s) \\ \vdots \qquad\quad \vdots \\ k(\mathbf{x}_s, \mathbf{x}_1) \ldots k(\mathbf{x}_s, \mathbf{x}_s) \end{bmatrix}$$

Here

$$m(\mathbf{x}) = E(f(\mathbf{x}))$$

and

$$k(\mathbf{x}, \mathbf{x'}) = E((f(\mathbf{x}) - m(\mathbf{x}))(f(\mathbf{x'}) - m(\mathbf{x'}))).$$

The Gaussian process will be denoted

$$f(\mathbf{x}) \sim \mathcal{GP}(m(\mathbf{x}), k(\mathbf{x}, \mathbf{x'}))$$

This means that the GP associates to each value of the input vector, namely any pair (SOC, I), a Gaussian probability distribution characterizing the voltage distribution at that point.

Usually, for notational simplicity, the mean function is set to zero [15]. The covariance function or kernel can be chosen from a wide set of possibilities. Given the smoothness of the recorded voltage versus SOC curves, the squared exponential kernel defined as

$$k_{SE} = \sigma^2 e^{-\frac{(x-x')^2}{2l^2}}, \tag{5}$$

appears to be an adequate choice, because it captures well smooth functions. The selection of the hyper-parameter vector θ = {σ,l} will be addressed below.

Considering the measurement noise on the voltage measurement, the regression model exploiting the GP can be written:

$$V = f(\mathbf{x}) + \xi$$

where ξ is assumed to be an independent identically distributed Gaussian noise with zero mean and variance σ_ξ^2. A Bayesian framework is used to predict the OCV associate to $I = 0$ by exploiting a set of s noisy output measurements gathered in vector $\mathbf{V}$ and associated to the input points $\mathbf{X}$ (training set). Let $\mathbf{X}_0$ and $\mathbf{f}_0$ denote respectively the matrix of input points at which the prediction is sought (test set) and the associated predictive distribution. The joint probability distribution associated to the training points and the test points can be written:

$$\begin{bmatrix} \mathbf{V} \\ \mathbf{f}_0 \end{bmatrix} \sim \mathcal{N}\left(\mathbf{0}, \begin{bmatrix} \mathbf{K_f}(\mathbf{X},\mathbf{X}) + \sigma_\xi^2\mathbf{I} & \mathbf{K_f}(\mathbf{X},\mathbf{X}_0) \\ \mathbf{K_f}(\mathbf{X}_0,\mathbf{X}) & \mathbf{K_f}(\mathbf{X}_0,\mathbf{X}_0) \end{bmatrix}\right) \tag{6}$$

The prediction is obtained by computing the conditional distribution of $\mathbf{f}_0$ given $\mathbf{X}, \mathbf{V}$ and $\mathbf{X}_0$ which is given as [15]

$$\mathbf{f}_0|\mathbf{X},\mathbf{V},\mathbf{X}_0 \sim \mathcal{N}(\bar{\mathbf{f}}_0, cov(\mathbf{f}_0)) \tag{7}$$

where

$$\bar{\mathbf{f}}_0 \equiv E(\mathbf{f}_0|\mathbf{X},\mathbf{V},\mathbf{X}_0) = \mathbf{K_f}(\mathbf{X}_0,\mathbf{X})\left[\mathbf{K_f}(\mathbf{X},\mathbf{X}) + \sigma_\xi\mathbf{I}\right]^{-1}\mathbf{V}$$

$$cov(\mathbf{f}_0) = \mathbf{K_f}(\mathbf{X}_0,\mathbf{X}_0) - \mathbf{K_f}(\mathbf{X}_0,\mathbf{X})\left[\mathbf{K_f}(\mathbf{X},\mathbf{X}) + \sigma_\xi\mathbf{I}\right]^{-1}\mathbf{K_f}(\mathbf{X},\mathbf{X}_0)$$

The predicted OCV curve is now characterized by a distribution of functions, which can be described for the i^{th} prediction input point as:

$$\widehat{OCV}_i = \bar{\mathbf{f}}_{0,i} \pm \sqrt{cov(\mathbf{f}_0)_{i,i}}h \tag{8}$$

where $\bar{\mathbf{f}}_{0,i}$ is the i^{th} element of $\bar{\mathbf{f}}_0$, $cov(\mathbf{f}_0)_{i,i}$ is the i^{th} diagonal element of the covariance matrix and constant h has to be adjusted according to the considered level for the confidence interval.

The hyper-parameters θ = {σ,l} from the kernel k(**x**,**x'**) and the process noise variance σ_ξ^2 must be estimated before exploiting the above expression (7), (8). It was done using a gradient descent method on the log marginal likelihood $\log\ p(\mathbf{V}|\mathbf{X},\theta,\sigma_\xi^2)$ [16].

III. Experimental setup

The experiments to gather the required data for comparing the performance, in terms of experimental time needed and prediction error, of the methods described in Section II, were carried out using 3 US18650VTC6 (3000mAh NCA/Graphite+Si) and 3 INR18650-30Q (3000mAh NCA/Graphite+Si) battery cells in an Arbin LBT21084 battery tester of 0 - 20V$\pm$2mV and 10A $\pm$0.2mA (4 current ranges 10A/500mA/20mA/1mA) per channel. To ensure reproducible conditions, the cells were tested at a constant ambient temperature, 25 ± 0.5^oC, within a PHCbi MIR-154-PE cooled incubator.

By reason of ensuring fairly equal initial conditions to gather the required data, the cells were subject to 5 cycles of charge and discharge with a low current (C/3) between 2.5 and 4.2V, before carrying out the experimental campaign. After this "activation" to ensure equal conditions, the cells were subject to a testing regime consisting of charges and discharges between 2.5 and 4.2V with increasing (dis)charging currents: C/100, C/50, C/20, C/10 and C/5. Such minimum and maximum voltage limits were taken from datasheet of the manufacturers [17] [18]. The experimental current and voltage profiles following such a testing regime are reported in Fig. 1 and Fig. 2, respectively.

At this point, to avoid comparing voltage curves with different time scales, Coulomb-counting method is used to estimate the relative electric State of Charge (SOC) of the battery at each i-th sampling point, for a constant current with magnitude I_j

$$\mathrm{SOC}_i = \frac{i\Delta T I_j}{\mathrm{Q}} \tag{9}$$

where ΔT is the sampling time, equal to 1s in this work, and Q is the nominal capacity of US18650VTC6 and INR18650-30Q cells in Ah, i.e., 3Ah. Next, to obtain equidistant points with respect to SOC, cubic spline interpolation is used.

The resulting Voltage-SOC curves for one US18650VTC6 cell are depicted in Fig. 3. Note that, for the sake of a fair comparison between the charge and discharge voltage curves, $\mathrm{SOC} = 0$ is assumed at the minimum voltage, i.e., $\mathrm{V_{min}} = 2.5V$.

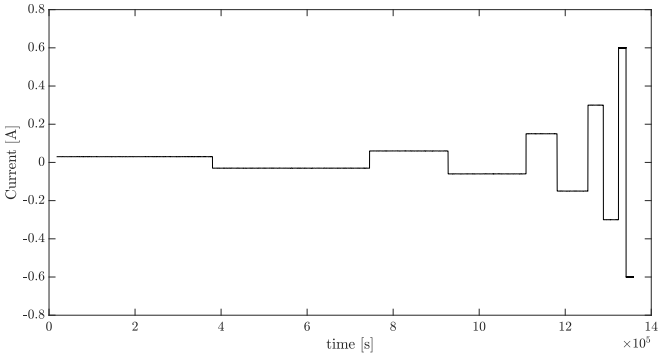

Fig. 1. Current profile of data acquisition (Sony VTC6 #1)

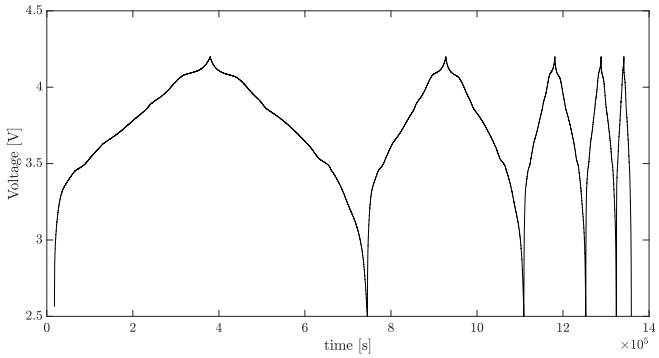

Fig. 2. Voltage profile of data acquisition (Sony VTC6 #1)

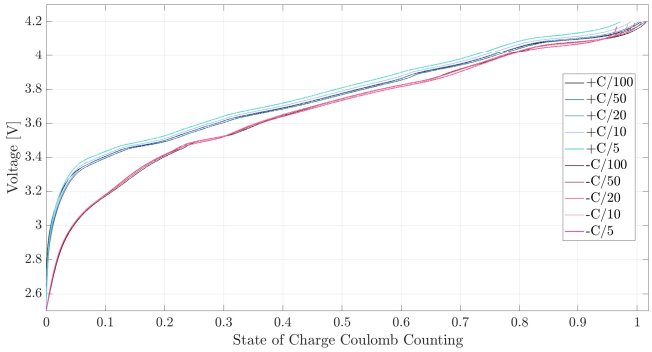

Fig. 3. Voltage-SOC curves for different applied currents (Sony VTC6 #1)

IV. Experimental Comparison of OCV-determination approaches

The Karhunen-Loève expansion (KLE) and Gaussian process regression (GPR) methods have been applied considering different combinations of charge/discharge curves. Every possible combination of the C-rates $\pm\{$C/50, C/20, C/10, C/5$\}$ has been considered. The same set of C-rate amplitudes is used for charge and discharge within each experiment. Although voltage curves for C-rate C/100 were available, they were only used for comparison in order to reduce the experimental time needed. The Root-Mean-Square Error (RMSE) metric has been selected to assess the performance of the algorithms. The error is computed between the resulting extrapolated OCV and the average of C/100 charge and discharge curves, that is used as a benchmark in this work.

From each signal, 300 samples have been considered for both methods. The samples are evenly distributed along the SOC span for the KLE method. The GPR method showed better results taking 40% of the sample in the 0-0.2 SOC range, 20% between 0.2 and 0.8 SOC and 40% from 0.8 to the maximal SOC. The maximal value of SOC considered is the biggest SOC value obtained during acquisition of the voltage curve with the highest C-rate in the set of curves used. The computation were done using the MATLAB software with a computer with 40GB of ddr4 RAM and a processor AMD Ryzen 7 5700U.

The RMSE resulting from both methods are shown in Fig. 4 and Fig.5. The dashed line represents the RMSE induced by using the averaged curve between charge and discharge at a C-rate of C/100 as the OCV instead of polarization-specific curves. The error presented is the average RMSE for the 3 batteries of the same kind (US18650VTC6 or INR18650-30Q) while using the same method and set of voltage curves.

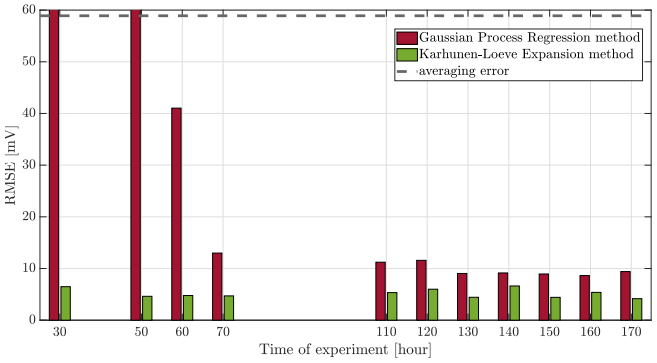

Fig. 4. mean RMS errors between extrapolated OCVs and the mean of C/100 charge and discharge curves (Sony VTC6)

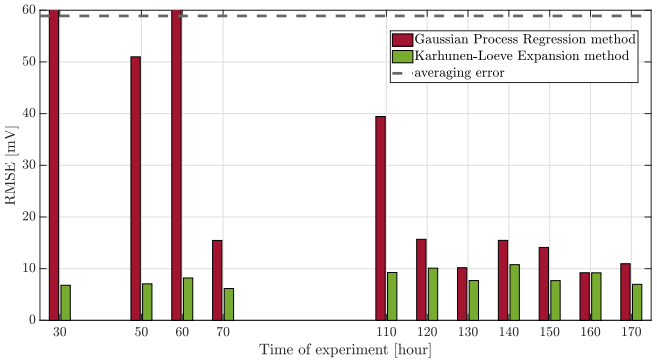

Fig. 5. mean RMS errors between extrapolated OCVs and the mean of C/100 charge and discharge curves (Samsung 30Q)

Both the Karhunen-Loève expansion (KLE) and Gaussian process regression (GPR) methods yield promising results, demonstrating errors significantly lower than the error induced by the averaging process of the C/100 curves. This suggests that the utilization of techniques designed to reduce the experimental time required for OCV acquisition does not introduce a greater error than disregarding the hysteresis phenomenon resulting from the battery polarization change. It is worth to emphasize that the error arising from neglecting the hysteresis phenomenon and the error presented in Fig. 4 do not aggregate. The former error is symmetric in both modes of battery use, namely charge and discharge, while the latter indicates a deviation from this symmetry. For instance, in Fig. 6, the extrapolated OCV obtained using the GPR approach consistently falls slightly below the mean OCV. This implies that SOC estimation would be slightly more accurate during discharge than charge, as the error between the discharge curve and the extrapolated curve is lower compared to the charge curve.

Comparing the errors introduced by the two methods, the KLE approach consistently outperforms the GPR approach. While the difference between the two methods is low for higher time of experiment, the GPR method seems unsuited when considering higher C-rate experiments. For the dataset used in this work, the selection of experimental voltage curves for the GPR must contain the $\pm$ C/50 curves or contain at least 6 curves (3 of charge and 3 of discharge) in order to draw satisfying results. In contrast, the choice of experimental curves is less critical for the KLE method.

The best trade-off between the error introduced and the required experimental time is different for the KLE and for the GPR approaches. Good results can be obtained from the KLE method using the curves at C-rates $\pm\{$C/10, C/5$\}$, which requires approximately 30h in total, i.e., two times 10h (C/10) and 5h (C/5). The error introduced is only slightly worse than the lowest error achievable (at 170h of experimental time) with this method, while greatly reducing the experimental time. On its side, the best GPR results are achieved when using curves at C-rates $\pm\{$C/20, C/10, C/5$\}$. The resulting OCV with its 68% confidence bound is shown in Fig. 6. This reduces the required experimental time to about 70h, i.e., two times 20h, 10h and 5h for C/20 C/10 and C/50, respectively.

Furthermore, the results obtained from the KLE approach exhibit greater consistency between different battery types, as can be seen on Fig. 4 and Fig. 5. The results are slightly poorer for the Samsung 30Q cells, indicating that the quality of the extrapolation might be impacted by the chemistry of the battery cell.

The confidence bound estimated with the GPR method is promising, the benchmark lying mostly within the bound, as it can be seen for example in Fig. 6. A discrepancy only occurs at very low SOC. Depending on the application, an estimation of moderately poorer quality, as obtained by GP instead of PCA, but providing a confidence bound of good quality might be privileged.

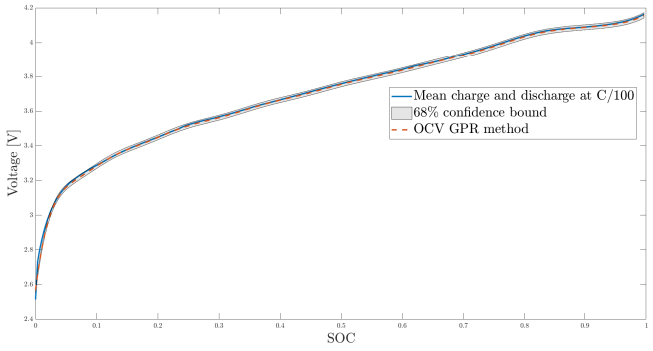

Fig. 6. mean of C/100 charge and discharge curves and extrapolated OCV using the GPR method with curves at C-rates C/20 and C/50 (Sony VTC6 battery #2)

V. Conclusion

The implementation of either of the two methods, Karhunen-Loève expansion or Gaussian process regression, represents a significant reduction of the experimental time required to characterize the OCV curve, Whereas the benchmark method requires approximately 200h for obtaining the constant-current charge and discharge curves at a C/100 C-rate, the GPR and KLE methods reduce the required time by 65% and 85%, respectively. This means that in the case of the KLE method, the standalone testing time of the battery can be reduced from more than 1 week to just 2 days, thus saving time and reducing the energy consumption of the testing equipment. Furthermore, the required testing equipment need not be extremely precise since the working current range is higher than for the benchmark case. For instance, for a 3000mAh US18650VTC6 cell, instead of working in the range of 30mAh (C/100), the implementation of the KLE approach allows working in the range of 300-600mAh (C/10-C/5), where the precision and the current control of the equipment can be slightly worse without compromising the quality of the curves obtained. The requirement of a testing device with a lower precision helps to reduce the purchase, procurement and calibration costs of the facilities where the tests have to be carried out.

Future research will involve a deeper exploration of the results variability, performing validation with battery cells from other manufacturers (e.g. LG) in order to assess the potential impact of the chemistry of the battery on the determination method. The evolution of the error when using higher C-rate curves will also be studied. In addition, the comparison study will be enhanced by considering data from the voltage relaxation method as well.

References

[1] Y. Wang, H. Fang, L. Zhou and T. Wada, Revisiting the state-of-charge estimation for lithium-ion batteries: a methodical investigation of the extended Kalman filter approach, IEEE control systems magazine, vol. 37, no. 4, pp. 73-96, 2017.

[2] L. D. Couto, J. Schorsch, M. M. Nicotra and M. Kinnaert, SOC and SOH estimation for Li-ion batteries based on an equivalent hydraulic model. Part I: SOC and surface concentration estimation, American Control Conference (ACC), pp. 4022-4028, 2016.

[3] L. D. Couto, S. M. Schons, D. Coutinho and M. Kinnaert, A descriptor system approach for the nonlinear state estimation of li-ion battery series/parallel arrangements, IEEE Transactions on Control Systems Technology, vol. 31, no. 2, pp. 825-840, 2023.

[4] Y. Zou, X. Hu, H. Ma, S. E. Li, Combined state of charge and state of health estimation over lithium-ion battery cell cycle lifespan for electric vehicles, Journal of Power Sources, Volume 273, pp. 793-803, 2015.

[5] G. L. Plett, Battery Management Systems Volume I Battery Modeling, Artech House Publishers, 2015.

[6] V. Pop, H. Jan Bergveld, D. Danilov, P. P. L. Regtien and P. H. L. Notten, Battery Management Systems Accurate State-of-Charge Indication for Battery-Powered Applications, Springer, 2008.

[7] I. Snihir, W. Rey, E. Verbitskiy, A. Belfadhel-Ayeb and P. H.L. Notten, Battery open-circuit voltage estimation by a method of statistical analysis, Journal of Power Sources, vol. 159, no. 2, pp. 1484-1487, 2006.

[8] M. Doyle and Y. Fuentes, Computer simulations of a Lithium-Ion polymer battery and implications for higher capacity next-generation battery designs, Journal of The Electrochemical Society, vol. 150, no. 6, pp. A706-A713, 2003.

[9] S. Santhanagopalan, Q. Guo and R. E. White, A Parameter estimation and model discrimination for a Lithium-Ion cell, Journal of the Electrochemical Society, vol. 154, no. 3, pp. A198-A206, 2007.

[10] H. J. Bergveld, W. S. Kruijt, and P. H. L. Notten, Battery management systems, Battery Management Systems, Springer, pp. 9-30, 2002.

[11] G. L. Plett, Extended Kalman filtering for battery management systems of LiPB-based HEV battery packs: Part 2. Modeling and identification, Journal of power sources, Elsevier, vol. 134, no. 2, pp. 262-276, 2004.
[12] V. Srinivasan, J. W. Weidner and J. Newman, Hysteresis during cycling of nickel hydroxide active material, Journal of the Electrochemical Society, vol. 148, no. 9, p. A969, 2001.
[13] G. Dong, J. Wei, and C. Zhang and Z. Chen, Online state of charge estimation and open circuit voltage hysteresis modeling of LiFePO4 battery using invariant imbedding method, Applied Energy, Elsevier, vol. 162, pp. 163-171, 2016.
[14] A. Barai, W. D. Widanage, J. Marco, A. McGordon, P. Jennings, A study of the open circuit voltage characterization technique and hysteresis assessment of lithium-ion cells, Journal of Power Sources, Elsevier, vol. 295, pp. 99-107, 2015.
[15] Rasmussen, C.E. and Williams K.I., Gaussian Processes for Machine Learnings, MITPress, 2006.
[16] E. Schulz, M. Speekenbrink and A. Krause, A tutorial on Gaussian process regression: Modelling, exploring, and exploiting functions, Journal of Mathematical Psychology, Academic Press Inc., vol. 85, pp. 1-16, 2018.
[17] Lithium Ion Rechargeable Battery Technical Information Model Number US18650 Revision 0.2, Sony Energy Devices Corporation, 2015
[18] Lithium-ion Rechargeable Cell for Power Tools Model Name INR18650-30Q Revision 1.0, Samsung SDI Co., Ltd. Energy Business Division, 2015